ACS APPLIED MATERIALS & INTERFACES

Research Article

www.acsami.org

Facile Fabrication of PEDOT:PSS/Polythiophenes Bilayered Nanofilms on Pure Organic Electrodes and Their Thermoelectric Performance

Hui Shi,‡ Congcong Liu,‡ Jingkun Xu,* Haijun Song, Baoyang Lu, Fengxing Jiang, Weiqiang Zhou, Ge Zhang, and Qinglin Jiang

Jiangxi Key Laboratory of Organic Chemistry, Jiangxi Science and Technology Normal University, Nanchang 330013, China

ABSTRACT: A pure organic PEDOT:PSS nanofilm was used as a working electrode for the first time to electrodeposit polymer films of polythiophene (PTh) and its derivatives in a boron trifluoride diethyl ether (BFEE) solution, fabricating a novel generation of bilayered nanofilms. Cyclic voltammetry (CV) demonstrated good electrochemical stability of the as-formed films. Structures and surface morphologies were systematically investigated by the characterizations of cross-section SEM, FT-IR, UV−vis, SEM, and AFM. The resulting films revealed stable and enhanced thermoelectric (TE) performances. The electrical conductivity values of PEDOT:PSS/PTh, PEDOT:PSS/P3MeT, and PEDOT:PSS/P3HT nanofilms were determined to be 123.9, 136.5, and 200.5 S cm^{-1}, respectively. The power factor reached up to be a maximum value of 5.79 $\mu W\ m^{-1}\ k^{-2}$. Thus, this technique offers a facile approach to a class of bilayered nanofilms, and it may provide a general strategy for fabricating a new generation of conducting polymers for more practical applications.

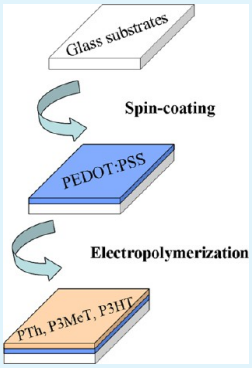

KEYWORDS: *PEDOT:PSS nanofilm, working electrode, polythiophene, bilayered nanofilms, thermoelectric performance*

1. INTRODUCTION

Materials that combine optical, electrical, and thermal properties, such as conducting polymers, are scientifically interesting as well as technologically useful.[1,2] In spite of their relatively short history, conducting polymers have been of particular significance in specialized industrial applications,[3] including solar cells, light-emitting diodes, sensors, electrodes, super capacitors, thermoelectric (TE) materials, and so forth.[4−9]

Up to now, a large amount of work has been devoted to the fundamental research[10] and applications of conducting polymers. Among the family of conducting polymers, polythiophene (PTh), and its derivatives such as poly(3-methylthiophene) (P3MeT), poly(3-hexylthiophene) (P3HT), and poly(3,4-ethylenedioxythiophene) (PEDOT) have attracted the greatest interest.[11−15] Dlaz et al.[11] first synthesized PTh through electrochemical polymerization, one of the fastest and most reliable conventional synthetic methods, and the films exhibited high electrical conductivity. Then, Shi et al.[16] put forward for the first time that the applied potential of electrochemical polymerization would be reduced and obtain high-quality films using boron trifluoride diethyl ether (BFEE) system. In order to improve the water-solubility of PEDOT, polystyrenesulfonate (PSS) was introduced to synthesize PEDOT:PSS, which possesses excellent stability, flexible mechanical properties, and high transparency.[17] Ouyang and co-workers have proven that the electrical conductivity of PEDOT:PSS films could increase by 3 orders of magnitude when secondarily doped with organic solvents such as dimethyl sulfoxide (DMSO), ethylene glycol (EG), tetrahydrofuran (THF), and dimethyl formamide (DMF),[18] some of which have also been reported by our group.[19,20] Groenendaal and co-workers have indicated that PEDOT:PSS films could be heated in air at 100 °C for over 1000 h with only a minimal change in conductivity.[21] On the basis of the existing research findings, it is considered that a secondary-doped PEDOT:PSS nanofilm with high electrical conductivity and stability is expected to be a potential material for electrodes.

Despite the progresses listed above, it is widely perceived that the design and synthesis of novel conducting polymers with unique structures and properties is still very necessary and significant. With the development of nanoscience and nanotechnology, and rapid progress in inorganic nanoscale materials and devices such as the recent report of nanogenerator by Wang,[22] intensive studies have focused on fabricating various kinds of nanostructure conducting polymers, for the beneficial characteristics derived from their small dimensions and high surface-to-volume ratios.[23] At the same time, numerous approaches have been put forward regarding the preparations of such polymers. Spin-coating techniques have been used to prepare PEDOT:PSS nanofilms.[24] Meanwhile, a vapor deposition process, interfacial polymerization, and seeding polymerization methods have also been introduced to fabricate nanomaterials.[25−27] The synthesized samples exhibited good properties such as high electrical conductivity that provided great potential advantages for optimization of the performances of organic devices.

Composite materials, especially with multilayer structures, are another type of novel materials, where the composite would

Received: April 1, 2013
Accepted: December 6, 2013
Published: December 6, 2013

 © 2013 American Chemical Society

ideally possess the advantages of each component. Not long ago, Liu et al.[28] obtained three-dimensional (3D) graphene/PPy via a convenient hydrothermal process, followed by in situ electrochemical polymerization of pyrrole, and this system appeared ideal for investigation in this study for applications in advanced actuator systems. Similarly, single-walled carbon nanotube (SWCNT)/PEDOT:PSS films were prepared,[29,30] and they concluded that the enhanced electrical conductivity was attributed to the synergistic interaction between the two components. Moreover, PPy/PTh/PPy trilayer films were electrochemically synthesized by successive oxidation of pyrrole in aqueous solutions and thiophene in BFEE solution.[31] When combining the multilayered structures with the nanostructure, the materials possessed better properties and a wider array of potential applications. For example, a simple and scalable method was described for fabricating 3D few-layer graphene/multiwalled carbon nanotube (MWNT) hybrid nanostructure on industrial-grade metal foam foils via a one-step ambient pressure chemical vapor deposition (APCVD) process,[32] which exhibiting numerous merits, indicating that this unique structure was promising for future energy storage applications.

It is known from inorganic semiconductors that a multilayered structure can improve the electrical performances by the quantum effect.[33] Herein, we posit that multilayered even other composites, especially nanostructure conducting polymers, will also exhibite similar properties. Until now, there have been few reports[34] on the preparation and TE performances of multilayer nanostructure composite conducting polymers. On the basis of our current knowledge, compared with inorganic materials, conducting polymers inherently possess advantages of potentially low cost due to plenty of carbon resources, scalable manufacturing, and easy processing into versatile forms.[34]

In the present work, a PEDOT:PSS nanofilm electrode was used to electrodeposit polymer films of PTh and its derivatives to fabricate PEDOT:PSS/PThs bilayered nanofilms. It was revealed that the PEDOT:PSS/PTh, PEDOT:PSS/P3MeT, and PEDOT:PSS/P3HT bilayered nanofilms possessed good electrochemical stability and enhanced TE performances. Additional properties of the as-formed nanofilms, such as structures and surface morphologies, were also investigated in detail through cross-section SEM, FT-IR, UV−vis, SEM, and AFM.

2. EXPERIMENTAL SECTION

Materials. PEDOT:PSS aqueous solution (PH1000; Baytron). Thiophene (99%; J&K Chemical Ltd.), 3-methylthiophene (99%; J&K Chemical Ltd.), 3-hexylthiophene (98%; J&K Chemical Ltd.), DMSO (analytical grade; Beijing Chemical Works), H_2SO_4 (95−98%; Beijing Chemical Works), and H_2O_2 (30%; Beijing Chemical Works) were used directly as received. BFEE (Beijing Changyang Chemical Plant) was purified by distillation and stored at −20 °C before use.

Preparation of PEDOT:PSS/Polythiophenes bilayered nanofilms. First, PEDOT:PSS/5% DMSO (herein referred to as PEDOT:PSS) nanofilms were prepared by spin-coating at a speed of 2000 r min^{-1}. Then, the as-formed PEDOT:PSS nanofilms were used as working electrodes for the electropolymerization of thiophene, 3-methylthiophene, and 3-hexylthiophene in the BFEE system to fabricate the bilayered structures.

Characterizations. The electrochemical properties were measured by a Model 263 potentiostat/galvanostat (EG&G Princeton Applied Research, Oakridge, TN) under the control of a computer. The thicknesses of the PEDOT:PSS and PEDOT:PSS/PThs nanofilms were measured with an F20 thin-film analyzer (Filmetrics, American). The F20 measures thin-film characteristics by reflecting light through the sample over a range of wavelengths. FT-IR and UV−vis absorption spectra were carried out using a Bruker Vertex 70 Fourier Transform Infrared Spectrometer and a Perkin-Elmer Lambda 900 UV−vis−near-infrared (NIR) spectrophotometer. SEM measurements were performed with a VEGA\\TESCAN scanning electron microscope, and cross-section SEM with a JEOL JSM-5600. The AFM measurements were operated on a NanoScope IIIa MultiMode in contact mode at room temperature under ambient conditions with commercially available etched silicon nitride probes. HMS-3000 was used to determine the carrier mobility and carrier concentration.

Before the TE measurements, samples of PEDOT:PSS and PEDOT:PSS/PThs nanofilms were cut into rectangular shape (length, 20.0 mm; width, 5.0 mm) and suspended by using a thermal paste between two thermoelectric devices (typically about 20 mm apart) used for creating a temperature difference. Electrical conductivity was measured by a homemade shielded four-point probe apparatus along with a Keithley 2700 Multimeter (Cleveland, OH) in conjunction with the Labview (National Instruments, Austin, TX) after four metal lines were patterned with silver paint. For the Seebeck coefficient measurement, a Keithley 2700 Multimeter (Cleveland, OH) and a regulated DC power supply (MCH-303D-∏, China) in conjunction with the Labview (National Instruments, Austin, TX) were utilized. Temperature gradients along the long edge of the sample were measured by two T-type thermocouples. A similar method has been reported by Kim et al.[35]

3. RESULTS AND DISCUSSION

The preparation process of the bilayered nanostructure films is shown in Schema 1. It contains the layer of glass substrates,

Scheme 1. Schematic Diagram of the Preparation of Bilayered Nanostructure Films

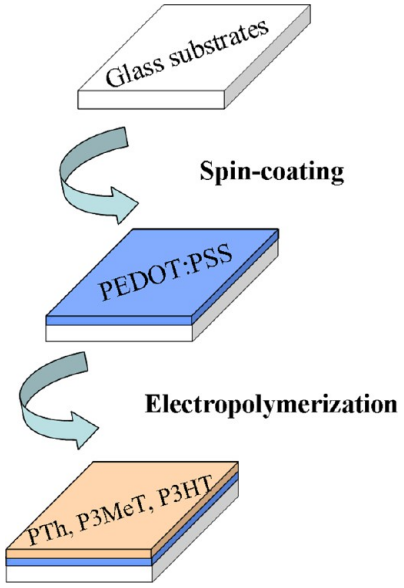

PEDOT:PSS nanofilms obtained via spin-coating techniques, and PTh (or P3MeT, P3HT) nanofilms prepared by electrochemical polymerization. The thickness of PEDOT:PSS films was 99 nm. The thicknesses of the PEDOT:PSS/PTh, PEDOT:PSS/P3MeT, and PEDOT:PSS/P3HT bilayer films were 175, 183, and 131 nm, respectively. The cross-section SEM images of (a) PEDOT:PSS, (b) PEDOT:PSS/PTh (c), PEDOT:PSS/P3MeT, and (d) PEDOT:PSS/P3HT films are shown in Figure 1. It may be not obvious enough to distinguish the boundaries. One reason is that the bilayered films are organic materials, and their composition is almost the same. Another reason is likely due to the process of electro-

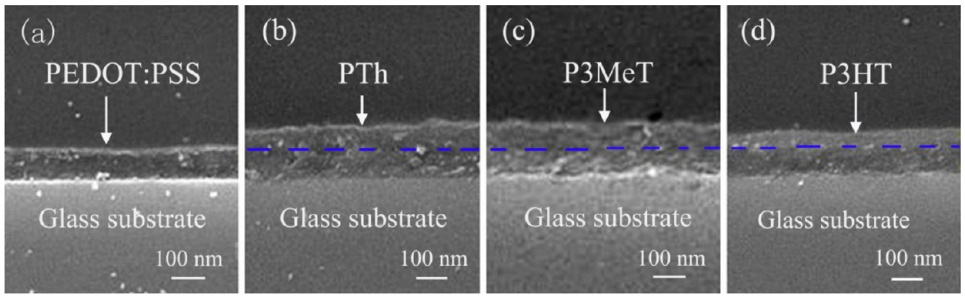

Figure 1. Cross-section scanning electron microscope (SEM) images of the nanofilms: (a) PEDOT:PSS, (b) PEDOT:PSS/PTh, (c) PEDOT:PSS/P3MeT, (d) PEDOT:PSS/P3HT.

polymerization, which formed a compact junction between the layers. Even so, when seen from the thickness, it is clear that the PThs have been deposited on the PEDOT:PSS electrodes, indicating the successful formation of bilayered structures.

The applied potential is one of the most significant parameters in an electrochemical polymerization process. In order to determine the proper conditions for electrochemical polymerization, the oxidation was carefully examined. Figure 2

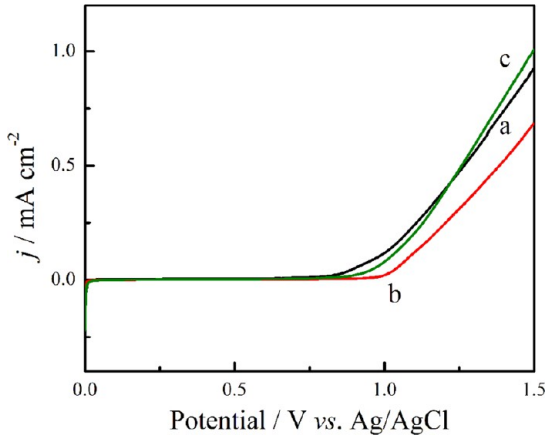

Figure 2. Anodic polarization curves of the monomers: (a) 0.025 M thiophene, (b) 0.05 M 3MeT, (c) 0.03 M 3HT. The potential scanning rate was 100 mV s^{-1}. *j* denotes the current density.

represents the anodic polarization curves of (a) 0.025 M thiophene, (b) 0.05 M 3-methylthiophene, and (c) 0.03 M 3-hexylthiophene in the BFEE system at a scanning rate of 20 mV s^{-1}. The onset oxidation potential was determined to be approximately 1.0, 0.95, and 0.9 V, respectively. As time went on, the PTh, P3MeT, and P3HT nanofilms were deposited on the electrodes, and the nanofilms obtained were used for all the characterizations mentioned below. At the same time, cyclic voltammetries (CVs) of the three monomers were investigated in the BFEE system, as shown in Figure 3. Successive potential scans of (a) thiophene, (b) 3-methylthiophene, and (c) 3-hexylthiophene led to the formation of the corresponding films. The increase in the anodic and cathodic peak current densities in the CVs implied that the amount of the polymer films increased on the surface of the electrodes.

The electrochemical behavior of the as-formed nanofilms was determined carefully in a monomer-free BFEE solution at scanning rates from 25 to 250 mV s^{-1}. As shown in Figure 4a, the CVs of the PEDOT:PSS nanofilm were performed over a wide range from −0.5 to +1.2 V, and the current densities increased as the scanning rate increased, showing the stability of

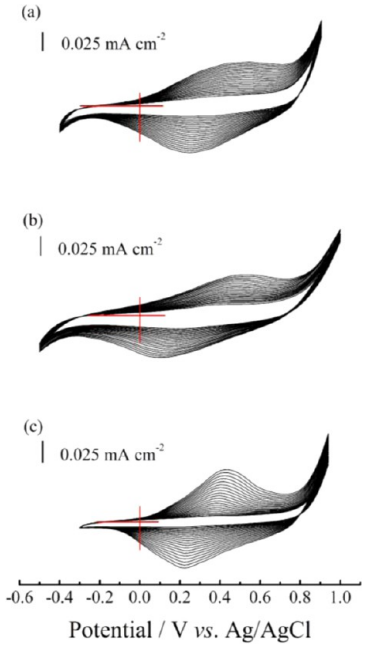

Figure 3. CVs of the monomers: (a) 0.25 M thiophene, (b) 0.5 M 3MeT, (c) 0.3 M 3HT in BFEE system. Potential scanning rate: 100 mV s^{-1}.

the PEDOT:PSS nanofilm electrodes in the BFEE system. Similarly, the CVs of the PEDOT:PSS/PTh (Figure 4b), PEDOT:PSS/P3MeT (Figure 4c), and PEDOT:PSS/P3HT (Figure 4d) nanofilms were tested over the potential ranges of −0.2 to +1.0 V, −0.2 to +1.0 V, and −0.05 to +0.9 V, respectively. The current densities increased with the increasing scanning rates. Broad anodic and cathodic peaks were presented,[36] and the peak current densities were proportional to the scanning rates (inset of Figure 3b−d), indicating the reversible redox behavior of the nanofilms. During the experiments, color changes were observed. Moreover, these nanofilms could be cycled repeatedly between the conducting (oxidized) and insulating (neutral) state without significant decomposition of the materials, indicating the high structural stability of the nanofilms.[31,37] On the basis of the previous discussion, it can be reasonably concluded that the electrode and the nanofilms that were electrochemically polymerized from BFEE exhibited good stability.

Several characteristic peaks are found in the PEDOT:PSS nanofilms, as shown in the inset of Figure 5A. The vibrations at 1316 and 1520 cm^{-1} are caused by the C−C and C═C stretching of the quinoidal structure and the ring stretching of the thiophene ring of the PEDOT chains. The band at about

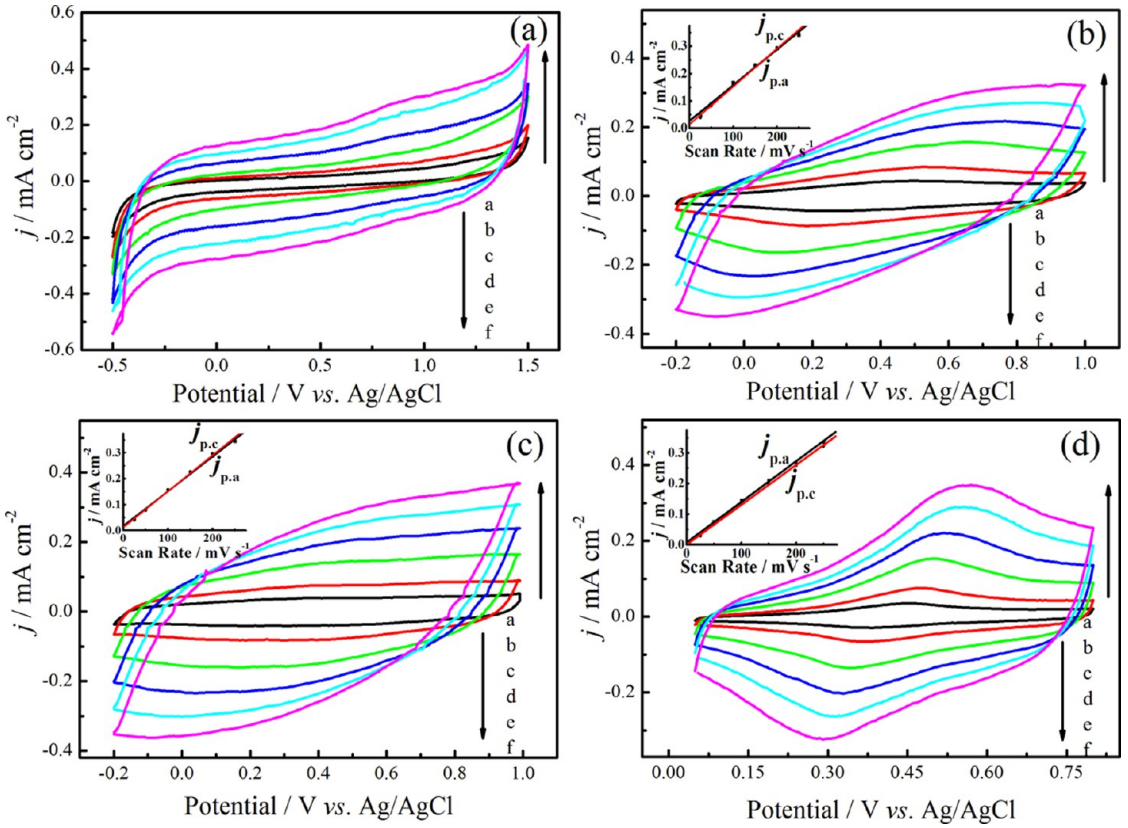

Figure 4. CVs of the samples: (a) PEDOT:PSS electrodes, (b) PEDOT:PSS/PTh nanofilms, (c) PEDOT:PSS/P3MeT nanofilms, and (d) PEDOT:PSS/P3HT nanofilms, recorded in the monomer-free BFEE solution at different potential scan rates. a−f refer to 25, 50, 100, 150, 200, and 250 mV s^{-1}. For the inset images, j is the current density, and $j_{p.a}$ and $j_{p.c}$ denote the anodic and cathodic peak current densities, respectively.

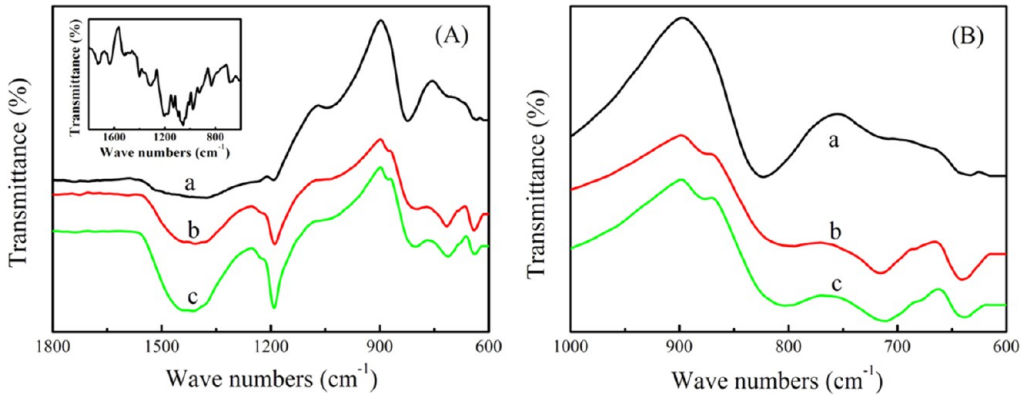

Figure 5. FT-IR spectra of the samples: (a) PEDOT:PSS/PTh, (b) PEDOT:PSS/P3MeT, (c) PEDOT:PSS/P3HT. The inset refers to PEDOT:PSS nanofilms.

831 cm^{-1} is related to the C−S bond vibration in the thiophene ring.[38] For the (a) PEDOT:PSS/PTh, (b) PEDOT:PSS/P3MeT, and (c) PEDOT:PSS/P3HT films in Figure 5A, the bands around 1426 and 1190 cm^{-1} are attributed to the C═C stretching vibration and the C−H bending of the thiophene ring. Although the band at about 715 cm^{-1} is assigned to C−S bending, and the band at 638 cm^{-1} is related to C−S−C ring deformation, which is in consistent with other literature reports.[39−41] As shown in Figure 5B with a narrow range from 600 to 1000 cm^{-1}, the band at 880 cm^{-1} for the PEDOT:PSS/P3MeT and PEDOT:PSS/P3HT films is related to $-CH_3$ terminal rocking,[42] which differs from PEDOT:PSS/PTh. Additionally, the C_β−H bending of the thiophene ring of the PEDOT:PSS/P3MeT and PEDOT:PSS/P3HT was located at 803 cm^{-1}, while it was located at 823 cm^{-1} for the PEDOT:PSS/PTh films, which maybe due to the $-CH_3$ and $-C_6H_{13}$ substituents on the thiophene ring.

The UV−vis absorption spectra (Figure 6) of the as-prepared nanofilms were studied carefully, and the measurements were carried out at room temperature in the wavelength range of 300 to 900 nm. The inset refers to the absorption of the PEDOT:PSS nanofilms, and there was an increasing absorbance after 500 nm. a, b, and c represent PEDOT:PSS/PTh, PEDOT:PSS/P3MeT, and PEDOT:PSS/P3HT nanofilms, respectively, which have respective maximum absorptions at 514, 462, and 507 nm. The current work showed good

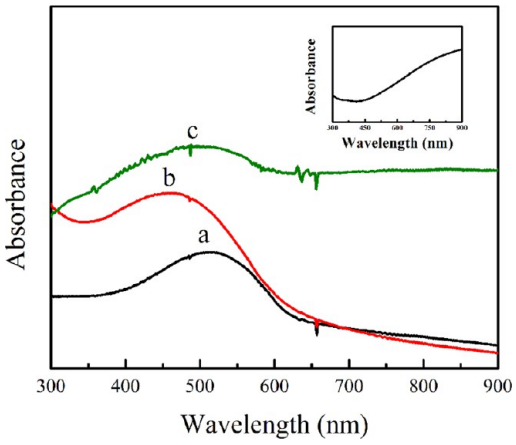

Figure 6. UV−vis absorption spectra of the samples: (a) PEDOT:PSS/PTh, (b) PEDOT:PSS/P3MeT, (c) PEDOT:PSS/P3HT. The inset refers to PEDOT:PSS nanofilms.

agreement with the literature results.[19,39,43] The values were all around 500 nm because of the $\pi-\pi^*$ (HOMO−LUMO) transition of the PTh backbones. Because the alkyl group was electron-donating, its presence can result in the reduction of electron density, which could make the average conjugation length became smaller. Thus, when −H of PTh was replaced by $-CH_3$ or $-C_6H_{13}$, the maximum absorption blue-shifted.

The SEM micrographs of PEDOT:PSS, PEDOT:PSS/PTh, PEDOT:PSS/P3MeT, and PEDOT:PSS/P3HT nanofilms are presented in Figure 7. For the PEDOT:PSS electrode (Figure 7a), the SEM image exhibited a uniform and smooth surface morphology. PTh (Figure 7b), P3MeT (Figure 7c) and P3HT (Figure 7d) films produced cauliflower-like, small grain-like, and particle-packing morphologies on the PEDOT:PSS electrodes, respectively. It was in consistent with previous reports.[20,39,43,44]

The two main parameters related to the TE performance, namely the electrical conductivity and Seebeck coefficient, were also carefully investigated. As for the electrode of PEDOT:PSS nanofilm, it possess an electrical conductivity of 393 S cm^{-1} and a Seebeck coefficient of 15 μV K^{-1}. Figure 8 displays the

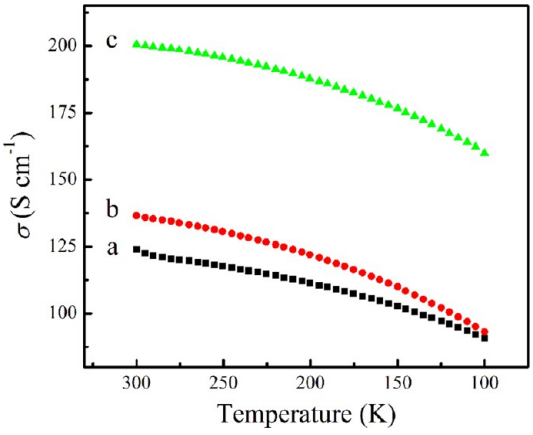

Figure 8. Temperature dependence of the electrical conductivity of the samples: (a) PEDOT:PSS/PTh, (b) PEDOT:PSS/P3MeT, (c) PEDOT:PSS/P3HT.

temperature dependence of the electrical conductivity over the temperature range of 300−100 K. It was found that the electrical conductivity of all the three samples decreased with the decreasing temperature, indicating a semiconductor behavior. The curve tendency of PEDOT:PSS/P3MeT was similar to that of PEDOT:PSS/P3HT, but was different from that of PEDOT:PSS/PTh, which might be due to the diversity

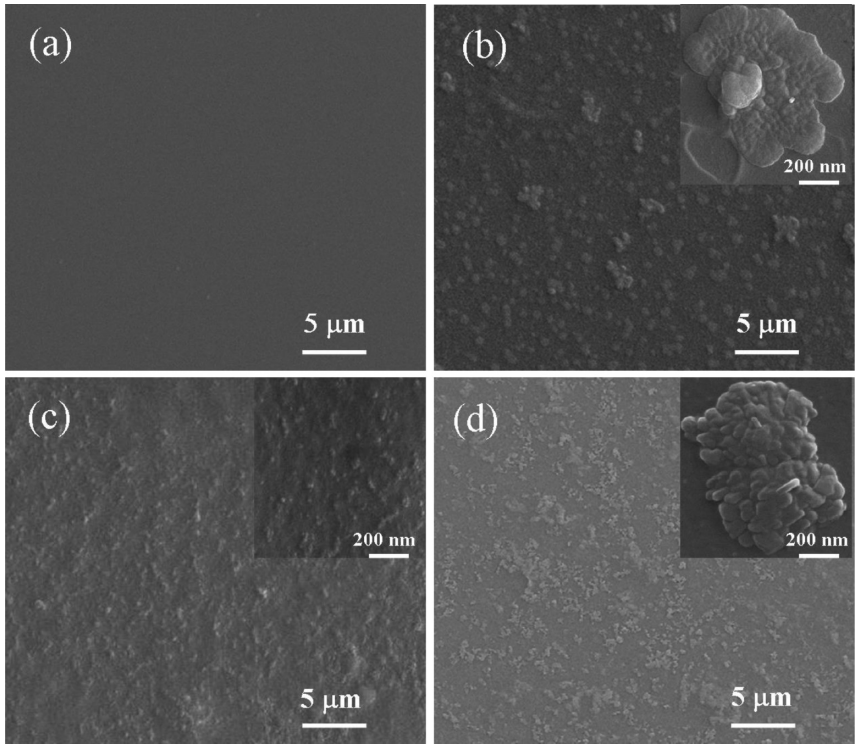

Figure 7. SEM images of the samples: (a) PEDOT:PSS electrode, (b) PEDOT:PSS/PTh, (c) PEDOT:PSS/P3MeT, (d) PEDOT:PSS/P3HT.

of their molecular structures. At 300 K, freshly prepared PEDOT:PSS/PTh nanofilms exhibited good electrical conductivity of 123.9 S cm^{-1}, whereas those of PEDOT:PSS/P3MeT and PEDOT:PSS/P3HT were as high as 136.5 and 200.5 S cm^{-1}. In our previous work, the PTh and P3MeT free-standing films prepared in the BFEE system exhibited the electrical conductivity of 46.1 and 98.5 S cm^{-1}.[43] Thus, the electrical conductivity of PEDOT:PSS/PTh and PEDOT:PSS/P3MeT in our present work was enhanced and preferable. Until now, there has been no report on the TE performance of P3HT obtained from a BFEE system. Xuan et al.[45] have systematically investigated the TE performance of P3HT, where the undoped P3HT showed the electrical conductivity around 1.67×10^{-5} S cm^{-1}, which is much lower than that of PEDOT:PSS/P3HT (200.5 S cm^{-1}). It has been reported that the substrate contribution to the electrical resistivity is considered negligible when the resistivity ratio between substrate and film is lager than 10000:1.[46] However, the electrical resistivity between the PEDOT:PSS-glass substrate and PThs films are of little differences. Thus, we consider that the high-conductive layer of PEDOT:PSS is beneficial for the electrical conductivity enhancement of the bilayered nanofilms.

The electrical conductivity can also be defined as $\sigma = en\mu$, where e, n, and μ are the electric charge, carrier concentration, and carrier mobility, respectively. The electrical conductivity is proportional to the carrier concentration and the carrier mobility.[47] The experimentally measured carrier mobility and carrier density are given in Table 1. The PEDOT:PSS nanofilms show the carrier mobility of 0.0168 $cm^2\ V^{-1}\ s^{-1}$. It was observed that the carrier mobility increases in the order of PEDOT:PSS/PTh, PEDOT:PSS/P3MeT, and PEDOT:PSS/P3HT nanofilms, with values of 0.07, 0.113, and 0.245 $cm^2\ V^{-1}\ s^{-1}$, respectively, which is in agreement with the electrical conductivity. The improvement of electrical conductivity is mainly considered to come from the carrier mobility enhancement.[48] It was also found that PEDOT:PSS nanofilms possess the highest carrier concentration of 4.62×10^{22} cm^{-3}, and the carrier concentration of the bilayered films does not change substantially when the carrier mobility dramatically increases.

Table 1. Characteristic Carrier Mobility, And Carrier Density at Room Temperature for PEDOT:PSS, PEDOT:PSS/PTh, PEDOT:PSS/P3MeT, and PEDOT:PSS/P3HT Nanofilms

samples	carrier mobility ($cm^2\ V^{-1}\ s^{-1}$)	carrier density (cm^{-3})
PEDOT:PSS	0.0168	4.62×10^{22}
PEDOT:PSS/PTh	0.07	8.2×10^{21}
PEDOT:PSS/P3MeT	0.113	4.46×10^{21}
PEDOT:PSS/P3HT	0.245	2.43×10^{21}

In addition, the atomic force microscope (AFM) results are exhibited in Figure 9. The spin-coated PEDOT:PSS nanofilms (a) with surface roughness value of 1.5 nm exhibit the most smooth and homogeneous morphology. After electropolymerization, PEDOT:PSS/PTh (b), PEDOT:PSS/P3MeT (c), and PEDOT:PSS/P3HT (d) bilayered films were obtained. Microscopically, the surface morphology significantly changed, showing the surface roughness values of 10.4, 18.7, and 20.4 nm. As mentioned above, the electrical conductivity of PEDOT:PSS/P3MeT is higher than that of PEDOT:PSS/PTh, but lower than that of PEDOT:PSS/P3HT, agreeing well with the corresponding surface roughness values.[24]

Figure 10 presents the temperature dependence of the Seebeck coefficient (S) over the temperature range of 200−300 K. For all the three samples, the values of the Seebeck coefficient were positive at room temperature, suggesting the presence of holes as majority carriers.[49] Meanwhile, the Seebeck coefficient decreased with the decreasing temperature, and the same behavior was observed for the electrical conductivity. At 300 K, the PEDOT:PSS/PTh nanofilms revealed a Seebeck coefficient of 11.2 $\mu V\ K^{-1}$, and those of PEDOT:PSS/P3MeT and PEDOT:PSS/P3HT were measured to be 18 and 17 $\mu V\ K^{-1}$. There is still much room for optimization of the Seebeck coefficient, and, therefore, the power factor. Further improvement is necessary to meet the needs of applications for TE materials.

For TE materials, it is often difficult to realize high electrical conductivity and high Seebeck coefficient at the same time. Meanwhile, it is considered difficult to enhance TE properties through composites, because early theoretical numerical simulations indicated that the Seebeck coefficient and the ZT value of the composites could not be higher than the maximum of one of its components.[50,51] Teehan et al.[52] have also reported that the resultant Seebeck coefficient of the multilayer structures is actually an intermediate between that of the two parent films it is composed of.

Researchers have revealed that the Seebeck coefficient is mostly governed by effective mass and carrier concentration.[53] Gao et al.[54,55] have reported that the Seebeck coefficient is very sensitive to the doping concentration, and the Seebeck coefficient of polythiophene decreases with the increase of the hole concentrations. Band-structure calculations indicate that materials with high Seebeck coefficient are often associated with very high density of states near the Fermi level.[54] Because there is a much higher density of states at the Fermi level in low-dimensional structures, three-dimensional (3D) materials, just like the bilayer nanofilms we fabricated tend to have inferior Seebeck coefficient than the 1D or 2D ones.[56]

In theory, the energy filtering effect connected to a potential barrier, which forms at the interface in semiconductors, is often regarded as a method for increasing the Seebeck coefficient in nanostructured materials.[57,58] In detail, when a large number of carriers hop together mainly in one direction, a process called energy filtering may arise,[59,60] where appropriate potential barriers at crystallite boundaries preferentially allow the carriers with higher energy to pass, thereby increasing the mean carrier energy in the flow, hence, the Seebeck coefficient. In addition, the Seebeck coefficient could be improved by the following methods: the metal/polymer/metal design,[61] antiresonant nanoparticle scattering,[62] or electron energy barrier filtering.[63] Our further investigation will be focused on the aspects mentioned above to obtain better properties.

Figure 11 shows the variation of the power factor (P) with temperature for all the samples, where P is equal to σS^2. At 300 K, PEDOT:PSS/PTh nanofilms revealed a power factor of 1.57 $\mu W\ m^{-1}\ k^{-2}$, whereas those of PEDOT:PSS/P3MeT and PEDOT:PSS/P3HT were 4.43 and 5.79 $\mu W\ m^{-1}\ k^{-2}$. Because of the square dependence of the power factor on the Seebeck coefficient, further improvement will be expected to occur with the improvement of the Seebeck coefficient. Further improvement in electrical conductivity and Seebeck coefficient could be achieved by tailoring the nanostructure scale of the conducting polymers,[64] allowing new opportunities to control electrical

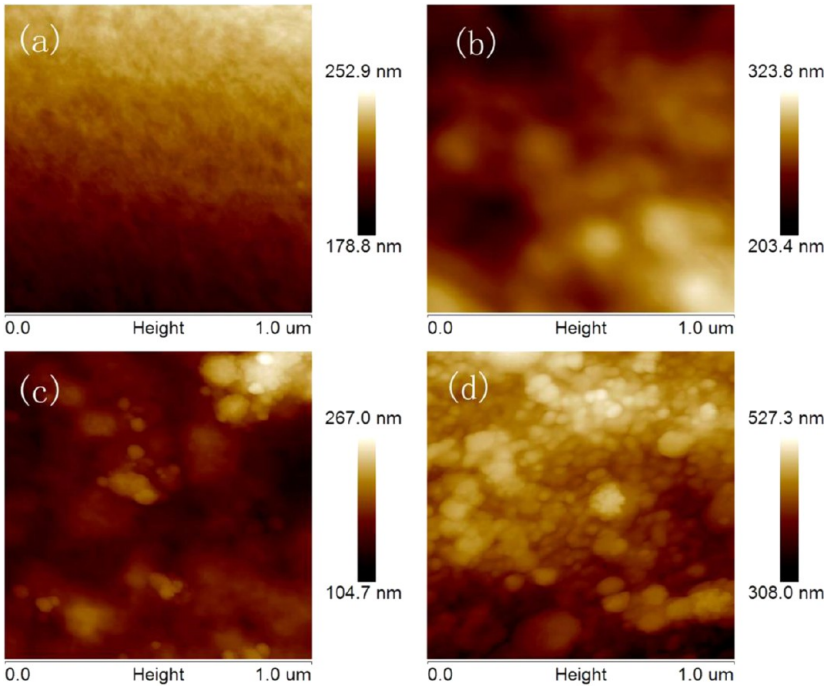

Figure 9. Atomic force microscopy (AFM) images of the samples: (a) PEDOT:PSS, (b) PEDOT:PSS/PTh, (c) PEDOT:PSS/P3MeT, (d) PEDOT:PSS/P3HT.

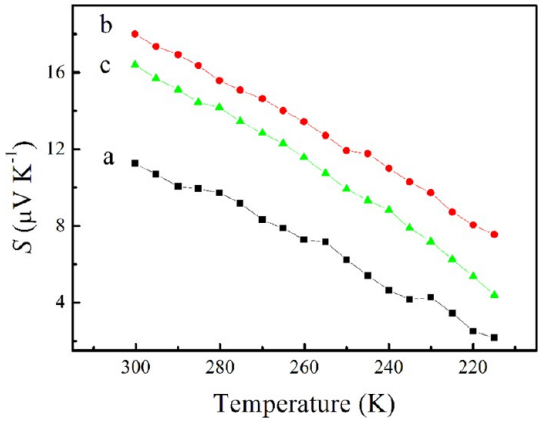

Figure 10. Temperature dependence of the Seebeck coefficient of the samples: (a) PEDOT:PSS/PTh, (b) PEDOT:PSS/P3MeT, (c) PEDOT:PSS/P3HT.

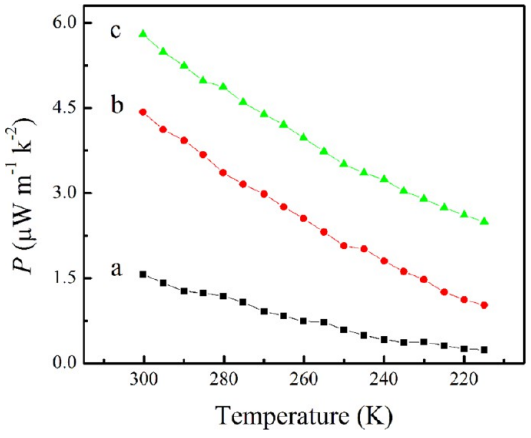

Figure 11. Temperature dependence of the power factor of the samples: (a) PEDOT:PSS/PTh, (b) PEDOT:PSS/P3MeT, (c) PEDOT:PSS/P3HT.

conductivity and Seebeck coefficient quasi-independently in order to improve the power factors and achieve better thermoelectric properties.[58]

4. CONCLUSIONS

In conclusion, a novel working electrode of PEDOT:PSS nanofilm with good electrochemical stability, homogeneous surface morphology, and high electrical conductivity was raised for the first time to electrodeposit PTh and its derivatives. A series of bilayered nanofilms of PEDOT:PSS/PTh, PEDOT:PSS/P3MeT, and PEDOT:PSS/P3HT were prepared based on PEDOT:PSS nanofilm electrodes in BFEE system. CVs demonstrated their good electrochemical stability in the monomer-free BFEE system. The structures and surface morphologies were systematically investigated. The bilayered nanostructure films exhibited TE properties of enhanced electrical conductivity and stable Seebeck coefficient, and their power factor reached a maximum of 5.79 μW m^{-1} k^{-2}. Most importantly, this approach may potentially be extended to prepare other materials systems such as PEDOT:PSS/PANI and PEDOT:PSS/graphene, or replace PEDOT:PSS with other conducting polymers, and provide a facile and general method for synthesizing materials with better TE performance for a wider array of applications.

AUTHOR INFORMATION

Corresponding Author

*E-mail: xujingkun@tsinghua.org.cn.

Author Contributions

‡Authors H.S. and C.L. contributed equally.The manuscript was written through contributions of all authors. All authors have given approval to the final version of the manuscript.

Notes

The authors declare no competing financial interest.

■ ACKNOWLEDGMENTS

This work was supported by National Natural Science Foundation of China (51203070 & 51073074) and Jiangxi Provincial Department of Education (GJJ12595 & GJJ11590 & GJJ13565).

■ ABBREVIATIONS

PTh, polythiophene
BFEE, boron trifluoride diethyl ether
CV, cyclic voltammetry
TE, thermoelectric
P3MeT, poly(3-methylthiophene)
P3HT, poly(3-hexylthiophene)
PEDOT, poly(3,4-ethylenedioxythiophene)
PSS, polystyrenesulfonate
DMSO, dimethyl sulfoxide
EG, ethylene glycol
THF, tetrahydrofuran
DMF, dimethyl formamide
3D, three-dimensional
SWCNT, single-walled carbon nanotube
APCVD, ambient pressure chemical vapor deposition

■ REFERENCES

(1) Rogers, J. A.; Someya, T.; Huang, Y. *Science* **2010**, *327*, 1603−1607.
(2) Dubey, N.; Leclerc, M. *J. Polym. Sci., Part B: Polym. Phys.* **2011**, *49*, 467−475.
(3) Shirakawa, H.; Louis, E. J.; Macdiarmid, A. G.; Chiang, C. K.; Heeger, A. J. *J. Chem. Soc., Chem. Commun.* **1977**, 578−580.
(4) Cheng, Y. J.; Yang, S. H.; Hsu, C. S. *Chem. Rev.* **2009**, *109*, 5868−5923.
(5) Gustafsson, G.; Cao, Y.; Treacy, G. M.; Klavetter, F.; Colaneri, N.; Heeger, A. J. *Nature* **1992**, *357*, 477−479.
(6) Taccola, S.; Greco, F.; Zucca, A.; Innocenti, C.; Fernández, C. J.; Campo, C.; Sangregorio, C.; Mazzolai, B.; Mattoli, V. *ACS Appl. Mater. Interfaces* **2013**, *5*, 6324−6332.
(7) Lee, T. H.; Do, K.; Lee, Y. W.; Jeon, S. S.; Kim, C.; Ko, J.; Im, S. S. *J. Mater. Chem.* **2012**, *22*, 21624−21629.
(8) Liu, R.; Duay, J.; Lane, T.; Lee, S. B. *Phys. Chem. Chem. Phys.* **2010**, *12*, 4309−4316.
(9) Sun, Y. M.; Sheng, P.; Di, C. A.; Jiao, F.; Xu, W.; Qiu, D.; Zhu, D. B. *Adv. Mater.* **2012**, *24*, 932−937.
(10) Campbell, D. K. *Synth. Met.* **2002**, *125*, 117−128.
(11) Wattman, R. J.; Bargon, J.; Diaz, A. F. *J. Phys. Chem.* **1983**, *87*, 1459−1463.
(12) Santoso, H. T.; Singh, V.; Kalaitzidou, K.; Cola, B. A. *ACS Appl. Mater. Interfaces* **2012**, *4*, 1697−1703.
(13) Shi, G. Q.; Xu, J. K.; Fu, M. X. *J. Phys. Chem. B* **2002**, *106*, 288−292.
(14) Bounioux, C.; Díaz-Chao, P.; Campoy-Quiles, M.; Martín-González, M. S.; Goñi, A. R.; Yerushalmi-Rozen, R.; Müller, C. *Energy Environ. Sci.* **2013**, *6*, 918−925.
(15) Taggart, D. K.; Yang, Y.; Kung, S. C.; Mcintire, T. M.; Penner, R. M. *Nano Lett.* **2011**, *11*, 125−131.
(16) Shi, G. Q.; Jin, S.; Xue, G.; Li, C. *Science* **1995**, *267*, 994−996.
(17) Yue, R. R.; Xu, J. K. *Synth. Met.* **2012**, *162*, 912−917.
(18) Ouyang, J. Y.; Xu, Q. F.; Chu, C. W.; Yang, Y.; Li, G.; Shinar, J. *Polymer* **2004**, *45*, 8443−8450.
(19) Liu, C. C.; Lu, B. Y.; Yan, J.; Xu, J. K.; Yue, R. R.; Zhu, Z. J.; Zhou, S. Y.; Hu, X. J.; Zhang, Z.; Chen, P. *Synth. Met.* **2010**, *160*, 2481−2485.
(20) Jiang, Q. L.; Liu, C. C.; Song, H. J.; Shi, H.; Yao, Y. Y.; Xu, J. K.; Zhang, G.; Lu, B. Y. *J. Mater. Sci.: Mater. Electron.* **2013**, *24*, 4240−4246.
(21) Groenendaal, L.; Jonas, F.; Freitag, D.; Pielartzik, H.; Reynolds, J. R. *Adv. Mater.* **2000**, *12*, 481−494.
(22) Hou, T. C.; Yang, Y.; Lin, Z. H.; Ding, Y.; Park, C.; Pradel, K. C.; Chen, L. J.; Wang, Z. *Nano Energy* **2013**, *2*, 387−393.
(23) Pecher, J.; Mecking, S. *Chem. Rev.* **2010**, *110*, 6260−6279.
(24) Xia, Y. J.; Ouyang, J. Y. *ACS Appl. Mater. Interfaces* **2010**, *2*, 474−483.
(25) Back, J. W.; Lee, S.; Hwang, C. R.; Chi, C. S.; Kim, J. Y. *Macromol. Res.* **2011**, *19*, 33−37.
(26) Huang, J. X.; Kaner, R. B. *J. Am. Chem. Soc.* **2004**, *126*, 851−855.
(27) Zhang, X. Y.; Manohar, S. K. *J. Am. Chem. Soc.* **2004**, *126*, 12714−12715.
(28) Liu, J.; Wang, Z.; Zhao, Y.; Cheng, H. H.; Hu, C. G.; Jiang, L.; Qu, L. T. *Nanoscale* **2012**, *4*, 7563−7568.
(29) Zhang, J.; Gao, L.; Sun, J.; Liu, Y. Q.; Wang, Y.; Wang, J. P. *Diamond Relat. Mater.* **2012**, *22*, 82−87.
(30) Zhou, J.; Lubineau, G. *ACS Appl. Mater. Interfaces* **2013**, *5*, 6189−6200.
(31) Han, G. Y.; Shi, G. Q. *Sens. Actuators, B* **2004**, *99*, 525−531.
(32) Wang, W.; Guo, S. R.; Penchev, M.; Ruiz, I.; Bozhilov, K. N.; Yan, D.; Ozkan, M.; Ozkan, C. S. *Nano Energy* **2013**, *2*, 294−303.
(33) Hicks, L. D.; Harman, T. C.; Dresselhans, M. S. *Appl. Phys. Lett.* **1993**, *63*, 3230.
(34) Toshima, N. *Macromol. Symp.* **2002**, *186*, 81−86.
(35) Kim, D.; Kim, Y.; Choi, K.; Grunlan, J. C.; Yu, C. *ACS Nano* **2010**, *4*, 513−523.
(36) Li, X. G.; Huang, M. R.; Duan, W. *Chem. Rev.* **2002**, *102*, 2925−3030.
(37) Lu, B. Y.; Xu, J.; Fan, C. L.; Jiang, F. X.; Miao, H. M. *Electrochim. Acta* **2008**, *54*, 334−340.
(38) Jian, J. M.; Guo, X. S.; Lin, L. W.; Cai, Q.; Cheng, J.; Li, J. P. *Sens. Actuators, B* **2013**, *178*, 279−288.
(39) Senthilkumar, B.; Thenamirtham, P.; Selvan, R. K. *Appl. Surf. Sci.* **2011**, *257*, 9063−9067.
(40) Galal, A. *J. Appl. Polym. Sci.* **2006**, *102*, 2416−2425.
(41) Kim, K.; Shin, J. W.; Lee, Y. B.; Cho, M. Y.; Lee, S. H.; Park, D. H.; Jiang, D. K.; Lee, J. K.; Joo, J. *ACS Nano* **2010**, *4*, 4197−4205.
(42) Feng, W.; Wan, A. S.; Garfunkel, E. *J. Phys. Chem. C* **2013**, *117*, 9852−9863.
(43) Hu, Y. J.; Shi, H.; Song, H. J.; Liu, C. C.; Xu, J. K.; Zhang, L.; Jiang, Q. L. *Synth. Met.* **2013**, *181*, 23−26.
(44) Goutam, P. J.; Singh, D. K.; Giri, P. K.; Iyer, P. K. *J. Phys. Chem. B* **2011**, *115*, 919−924.
(45) Xuan, Y.; Liu, X.; Desbief, S.; Leclère, P.; Fahlman, M.; Lazzaroni, R.; Berggren, M.; Cornil, J.; Emin, D.; Crispin, X. *Phys. Rev. B* **2010**, *82*, 115454.
(46) Manasreh, M. O.; Myers, T. H.; Julien, F. H. *Infrared Applications of Semiconductors−Materials, Processing, and Devices*, 2nd ed.; Wagner, A. V., Foreman, R. J., Farmer, J. C., Barbee, T. C., Eds.; Materials Research Society: Pittsburgh, PA, 1996; p 467−472.
(47) Hiroshige, Y.; Ookawa, M.; Toshima, N. *Synth. Met.* **2007**, *157*, 467−474.
(48) Yao, Q.; Chen, L. D.; Zhang, W. Q.; Liufu, S. C.; Chen, X. H. *ACS Nano* **2010**, *4*, 2445−2451.
(49) Lèvesque, I.; Gao, X.; Klug, D. D.; Tse, J. S.; Ratcliffe, C. I.; Leclerc, M. *React. Funct. Polym.* **2005**, *65*, 23−26.
(50) Bergman, D. J.; Levy, O. *J. Appl. Phys.* **1991**, *70*, 6821−6833.
(51) Lin-Chun, P. J.; Reinecke, T. L. *Phys. Rev. B* **1995**, *51*, 13244−13248.
(52) Teehan, S.; Efstathiadis, H.; Haldar, P. *J. Alloys Compd.* **2012**, *539*, 129−136.
(53) Kinemuchi, Y.; Nakano, H.; Mikami, M.; Kobayashi, K.; Watari, K.; Hotta, Y. *J. Appl. Phys.* **2010**, *108*, 053721.
(54) Gao, X.; Uehara, K.; Klug, D. D.; Patchkovskii, S.; Tse, J. S.; Tritt, T. M. *Phys. Rev. B* **2005**, *72*, 125202.

(55) Gao, X.; Uehara, K.; Klug, D. D.; Tse, J. S. *Comput. Mater. Sci.* **2006**, *36*, 49−53.
(56) Hicks, L. D.; Dresselhaus, M. S. *Phys. Rev. B* **1993**, *47*, 16631−16634.
(57) Poudel, B.; Hao, Q.; Ma, Y.; Lan, Y.; Minnich, A.; Yu, B.; Yan, X.; Wang, D.; Muto, A.; Vashaee, D.; Chen, X.; Liu, J.; Dresselhaus, M. S.; Chen, G.; Ren, Z. *Science* **2008**, *320*, 634−638.
(58) Dresselhaus, M. S.; Chen, G.; Tang, M. Y.; Yang, R.; Lee, H.; Wang, D.; Ren, Z.; Fleurial, J. P.; Gogna, P. *Adv. Mater.* **2007**, *19*, 1043−1053.
(59) Humphrey, T. E.; O'Dwyer, M. F.; Linke, H. *J. Phys. D: Appl. Phys.* **2005**, *38*, 2051−2054.
(60) Kima, R.; Lundstrom, M. S. *J. Appl. Phys.* **2012**, *111*, 024508.
(61) Stanford, M.; Wang, H.; Ivanov, I.; Hu, B. *Appl. Phys. Lett.* **2012**, *101*, 173304.
(62) Zebarjadi, M.; Liao, B.; Esfarjani, K.; Dresselhaus, M.; Chen, G. *Adv. Mater.* **2013**, *25*, 1577−1582.
(63) Zhao, L. D.; Hao, S. Q.; Lo, S. H.; Wu, C. I.; Zhou, X. Y.; Lee, Y.; Li, H.; Biswas, K.; Hogan, T. P.; Uher, C.; Wolverton, C.; Dravid, V. P.; Kanatzidis, M. G. *J. Am. Chem. Soc.* **2013**, *135*, 7364−7370.
(64) Meng, C. Z.; Liu, C. H.; Fan, S. S. *Adv. Mater.* **2010**, *22*, 535−539.